Modeling turbulence in UWOC based on Monte Carlo simulations

ZAHRA VALI,[1] ASGHAR GHOLAMI,[1,*] ZABIH GHASSEMLOOY,[2] DAVID G. MICHELSON,[3] MASOOD OMOOMI,[1] HAMED NOORI[3]

[1]*Optoelectronics and Optical Communications Research Laboratory (OOCRL), Department of Electrical and Computer Engineering, Isfahan University of Technology, Isfahan 84156-83111, Iran*
[2]*Optical Communications Research Group, NCR Lab, Northumbria University, Physical and Electrical Engineering Department, Newcastle upon Tyne, UK*
[3]*Radio Science Lab (RSL), Electrical and Computer Engineering Department, University of British Columbia, V6T 1Z4, 2332 Main Mall, Vancouver, BC, Canada*

**Corresponding author: gholami@cc.iut.ac.ir*

Received XX Month XXXX; revised XX Month, XXXX; accepted XX Month XXXX; posted XX Month XXXX (Doc. ID XXXXX); published XX Month XXXX

Turbulence affects the performance of underwater wireless optical communications (UWOC). Although multiple scattering and absorption have been previously investigated by means of physical simulation models, still a physical simulation model is needed for UWOC with turbulence. In this paper, we propose a Monte Carlo simulation model for UWOC in turbulent oceanic clear water, which is far less computationally intensive than approaches based on computational fluid dynamics. The model is based on the variation of refractive index in a horizontal link. Results show that the proposed simulation model correctly reproduces both lognormal and negative exponential probability density functions of the intensity fluctuations for weak and saturation turbulence regimes, respectively. Results presented match well with experimental data reported for weak turbulence. Furthermore, scintillation index and turbulence induced path loss versus link span are exhibited for different refractive index variations.

OCIS codes: *(010.4455) Oceanic propagation; (010.7060) Turbulence; (060.4510) Optical communications; (290.5930) Scintillation.*

http://dx.doi.org/10.1364/AO.99.099999

1. INTRODUCTION

Underwater wireless optical communications (UWOC) is an emerging high bandwidth, low time latency and highly secure technology compared to the radio frequency and acoustic based systems. UWOC is being investigated by researchers for scientific, environmental and commercial purposes in oceans in order to provide real-time communications among underwater vehicles and wireless sensor nodes [1]. In underwater environments both absorption and multiple scattering are the two important factors, which induce power loss, time dispersion (i.e., inter-symbol-interference (ISI)), leading to degraded link performance and reduced transmission spans (to < 100 m) as reported in the literature e.g. [2-5]. It is well known that seawater displays a relatively low loss property in blue and green lights (i.e. a transmission window of 450-550 nm) [6, 7], which has become the foundation for the development of future UWOC.

Turbulence is another factor which will have a significant impact on the link performance, thus further limiting the wide spread applications of UWOC. The propagation of laser beams through the atmospheric turbulence has been extensively investigated both theoretically and experimentally. However, laser beam propagation through the complex oceanic turbulence is a relatively unexplored area required detailed investigations. Turbulence is random variations of the refractive index of water n mainly due to the temperature and salinity fluctuations in ocean, which leads to the received intensity fluctuations or fading and beam spreading thus degrading the UWOC system performance[8, 9].

The irregular and unpredictable motions in oceans makes turbulence field testing challenging and experimentally costly and time consuming. Thus, there is a need for a simple simulation platform for predicting the system performance prior to any system design, implementation and evaluation. While prior studies have modeled and experimentally tested the absorption and multiple scattering phenomena [3-5], to the best of our knowledge there are no physical turbulence models of UWOCs. However, in the previous studies, various effects of turbulence on UWOC have been reported. In [10] the

effect of turbulence on the Gaussian beam waist over a 2 m water path was experimentally investigated. The effect of turbulence in the natural environment on underwater imaging was investigated experimentally in [11]. In [12] the index of refraction structure constant was experimentally investigated in clear water over a vertical transmission span of ~ 9 m. In [13] a Monte–Carlo based statistical simulation method was presented to characterize an UWOC channel with a single-input-multiple-output (SIMO) scheme under weak turbulence. The scintillation index (SI) values of plane, spherical and different Gaussian beams were obtained analytically in [14-16]. The SI and the bit-error-rate (BER) performance of higher order modes of laser beam in a horizontal UWOC link were evaluated under weak turbulence in [17] and [18], respectively. The SI and the corresponding BER performance of the multiple-input-single-output (MISO) UWOC system was quantified using laser beam array in [19].

In this paper, we focus on presenting a simple physical simulation model based on Monte Carlo method for a turbulent UWOC horizontal link, which is far less computationally intensive compared with the approaches based on computational fluid dynamics (CFD). The proposed model is based on the interaction of propagating photons with turbulent medium, which is presented in consecutive turbulent cells with different *n*. The variation of *n* is due to temperature, salinity and the pressure gradient. In addition, in this model we consider the effect of dynamic water flow on laser beam propagation.

In our model, the resultant intensity fluctuations of the received laser beam, is fitted with a closed-form expression of the probability density function (PDF). Knowing the PDF is essential in determining the reliability and the BER performance of UWOC systems [9, 20]. The three most reported closed form expression of intensity fluctuations for FSO link under weak, weak-to-strong and saturation turbulence regimes are log-normal, gamma–gamma and negative exponential, respectively [21]. However, not much research works have been reported on the PDF of intensity fluctuations for turbulent UWOC systems. A recent experimental work measuring PDF of the received laser beam power under weak turbulence in a 1 m water tank was reported in [22, 23]. The recent theoretical works, mainly focused on weak turbulence, have adopted the same PDF as the atmospheric turbulence (log-normal distribution) [13, 15, 18, 24-27]. However, no experimental and theoretical works have been reported information on the PDFs of moderate, strong and saturation turbulence regimes. Therefore, our new physical model is proposed to predict the PDF of the received laser beam power under different turbulence regimes. While the previous reported studies presented the dependence of SI on the fluid flow parameters in weak turbulence regime [14-16], in this model both the SI and the turbulence induced path loss are investigated based on the variation of *n*.

The rest of paper is organized as follows. In section 2 the concept of the simulation model is explained. Section 3 describes the structure of the simulation model. The verification and other simulation results are presented in section 4 and section 5 concludes the paper.

2. CONCEPT OF THE SIMULATION MODEL

Turbulence is the result of inevitable flow perturbations creating an unstable flow with large scale eddies [28]. These large eddies interact with each other, disperse their energy and form smaller eddies [29, 30]. Due to the chaotic nature of energy transfer from large to small eddies, the created turbulent eddies are homogeneous, isotropic and steady with different size each one has a constant *n* [21]. Therefore, in this work to model the turbulence, we have assumed a stratified water medium in the horizontal direction where each layer represents a homogenous and isotropic turbulent cell or eddy in the motion [31].

A. Refractive index variation

In order to define *n* in each turbulent cell, a distribution of *n* variation according to the oceanic water is needed. *n* will depend on the water pressure *P*, temperature *T*, salinity *S* and wavelength λ [31-33]. In the static waters, variations of *T*, *P* and *S* of water in small area are relatively minor. But in dynamic waters such as the real ocean environment, where turbulence is widely distributed, *n* changes rapidly in time and space. It is concluded from previous studies both in the oceanic water and in experimental conditions that *n* variation is assumed to occur randomly [9, 30, 34]. In our model, we present the fluctuations of *n* when considering *T*, *S* and *P* fluctuations using the refractive index equation which is well accepted for $0.5 < \lambda < 0.7$ μm, $0 < T < 30$ ℃, $0 < S < 43$ ppt and $0 < P < 11000$ dbar, as given by [32],

$$\begin{aligned} n(T,P,S,\lambda) = {} & n_0 + n_1\lambda^2 + n_2\lambda^{-2} + n_3\lambda^{-4} + n_4\lambda^{-6} \\ & + n_5T + n_6T^2 + n_7T^3 + n_8T^4 \\ & + (n_9T + n_{10}T^2 + n_{11}T^3)\lambda \\ & + (n_{12} + n_{13}\lambda^{-2} + n_{14}T + n_{15}T^2 + n_{16}T^3)S \\ & + n_{17}ST\lambda + n_{18}P + n_{19}P^2 + n_{20}P\lambda^{-2} \\ & + (n_{21}T + n_{22}T^2)P + n_{23}P^2T^2 \\ & + (n_{24} + n_{25}T + n_{26}T^2)PS. \end{aligned} \quad \textbf{(1)}$$

Note that, the coefficients in Eq. (1) can be found in [32]. For values of *T* and *S*, we have adapted the measured vertical profiles of temperature and salinity in the Florida Strait [30]. We have assumed that for the first 100 m of the *T* and *S* profiles, waters of different depth layers can be mixed together to create the turbulence. All the key system parameters, including *T* and *S* values adopted in the simulation are shown in Table 1.

3. THE STRUCTURE OF THE SIMULATION MODEL

The radiative transfer equation (RTE) is used to describe the behavior of light radiance generally in a three dimensional time-dependent inhomogeneous and anisotropic propagation medium [35]. Variation of *n* along the propagation path cause changes in time and space domain of the light intensity. Analytical solutions of RTE exist for simple cases, but for a more complex medium with turbulence effects it is rather challenging to obtain analytical solutions for the light intensity. Thus, we have adopted Monte Carlo method in developing a simulation model for UWOC in turbulent waters, which is simple and it can be readily modified for other communications scenarios. The proposed model is based on step-by-step tracing of a number of photons propagating within water from the transmitter (Tx) to the receiver (Rx).

The framework for the simulation model is a horizontal point-to-point three dimensional link in the *z*-direction. As part of the simulation we have made a number of assumptions including: (*i*) the propagation medium is infinite both in *x* and *y* directions in order to simulate the laser light transmission in the water; (*ii*) the interaction of light with the water-air surface is ignored for simplicity; and (*iii*) water is assumed to be clear with no particles and scattering and absorption do not exist. The Monte Carlo simulation model consists of three main parts: the Tx, channel and the Rx. The system block diagram is presented in Fig. 1 (a).

The Tx is a narrow-divergent optical Gaussian laser beam assumed to operate in the far-field region, which determines the position of each photon in the Cartesian coordinate by (x, y, z) and the direction of each photon being launched into the channel through direction cosines

$(\cos\theta x, \cos\theta y, \cos\theta z)$. θx, θy and θz are the angles between photon direction and x, y and z axes, respectively.

A. The turbulent channel

To simulate a turbulent channel, as shown in Fig. 1 (b), here we have made a number of assumptions: (*i*) m-layer with different n with each layer representing a turbulent cell [31]; (*ii*) curved boundaries separating adjacent turbulent layers; (*iii*) the i^{th} curved boundary between turbulent layers i and i+1 intercepts z axis at the position $\mathbf{P_i}(0, 0, z_i')$. $\mathbf{P_i}$ points are at constant positions with a Δz distance between consecutive points. Note that, m value depends on the total link span and Δz and Tx and Rx centers are situated on the z axis; (*iv*) the curved boundaries are assumed to be part of spheres with the radius R_i in three dimensional coordinates system. It will be explained later on that throughout simulation R_i is selected randomly within acceptable limit; and (*v*) the normal vector $\vec{\mathbf{n}}_\mathbf{i}$ at the $\mathbf{P_i}$ points is defined as,

$$\vec{\mathbf{n}}_\mathbf{i} = (a, b, c) = (\sin\theta_i \cos\varphi_i, \sin\theta_i \sin\varphi_i, \cos\theta_i) \quad \textbf{(2)}$$

in that, θ_i the polar angle is chosen randomly between zero and θ_{max} and φ_i the radial angle is chosen randomly in the interval of $[0, 2\pi]$ for i^{th} curved boundary. This implies the rotation of curved boundaries along the z direction.

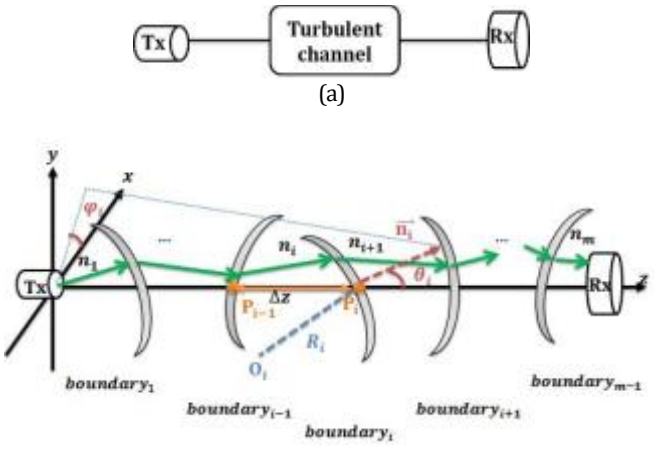

Fig. 1. (a) System block diagram, and (b) the consecutive boundaries with defined parameters in turbulent channel and interaction of a photon with them

B. Interaction of a photon with a boundary

Tracing photons movement within turbulent layers sequentially, the intersection point of each photon with each boundary $\mathbf{X_c}(x_c, y_c, z_c)$ is obtained simply through the intersection equations of a line and the boundary. If the photon has no intersection with the boundary, then the photon is marked as wasted photon and its trajectory calculation will be terminated. As shown in Fig. 2, the new direction of a photon following refraction from the i^{th} curved boundary is determined using the three dimensional Snell law in the vector form as given by,

$$\vec{\mathbf{L}}_{i+1} \times \vec{\mathbf{n}}_\mathbf{r} = \frac{n_i}{n_{i+1}} \vec{\mathbf{L}}_\mathbf{i} \times \vec{\mathbf{n}}_\mathbf{r}. \quad \textbf{(3)}$$

In Eq. (3), n_i and n_{i+1} are the refractive indices of i^{th} and i+1th layers, respectively. $\vec{\mathbf{L}}_\mathbf{i}$ and $\vec{\mathbf{L}}_\mathbf{i+1}$ are the directions of photon before and after interaction with the i^{th} boundary that are defined with the direction cosines as,

$$\vec{\mathbf{L}}_\mathbf{i} = (\mu_x, \mu_y, \mu_z) = (\cos\theta x_i, \cos\theta y_i, \cos\theta z_i), \quad \textbf{(4)}$$

$$\vec{\mathbf{L}}_{i+1} = (\mu_x', \mu_y', \mu_z') = (\cos\theta x_{i+1}, \cos\theta y_{i+1}, \cos\theta z_{i+1}). \quad \textbf{(5)}$$

$\vec{\mathbf{n}}_\mathbf{r}$ is the normal vector to the curved boundary in point $\mathbf{X_c}$ defined as,

$$\vec{\mathbf{n}}_\mathbf{r} = (a_r, b_r, c_r) = \frac{\overrightarrow{\mathbf{O_i X_c}}}{R_i} = \left(\frac{x_c - x_o}{R_i}, \frac{y_c - y_o}{R_i}, \frac{z_c - z_o}{R_i}\right), \quad \textbf{(6)}$$

where $\mathbf{O_i}(x_o, y_o, z_o)$ is the center of curved boundary. The three coplanar vectors of $\vec{\mathbf{L}}_\mathbf{i}$, $\vec{\mathbf{L}}_\mathbf{i+1}$ and $\vec{\mathbf{n}}_\mathbf{r}$ are satisfying the normalization condition to ensure that they are unit vectors,

$$\mu_x^2 + \mu_y^2 + \mu_z^2 = 1, \quad \textbf{(7)}$$

$$\mu_x'^2 + \mu_y'^2 + \mu_z'^2 = 1, \quad \textbf{(8)}$$

$$a_r^2 + b_r^2 + c_r^2 = 1. \quad \textbf{(9)}$$

At the first boundary, $\vec{\mathbf{L}}_\mathbf{i}$ is the incident direction of photon launched from the Tx and $\vec{\mathbf{L}}_\mathbf{i+1}$ is the refracted path direction, which is to be determined and will be updated as the $\vec{\mathbf{L}}_\mathbf{i}$ for the second boundary. While R_i is chosen randomly for each boundary, $\mathbf{O_i}$ is obtained through the normal vector $\vec{\mathbf{n}}_\mathbf{i}$ and the known point $\mathbf{P_i}$, which are given by,

$$\vec{\mathbf{n}}_\mathbf{i} = (a, b, c) = \frac{\overrightarrow{\mathbf{O_i P_i}}}{R_i}, \quad \textbf{(10)}$$

$$\mathbf{O_i} = (x_o, y_o, z_o) = (-aR_i, -bR_i, z_i' - cR_i). \quad \textbf{(11)}$$

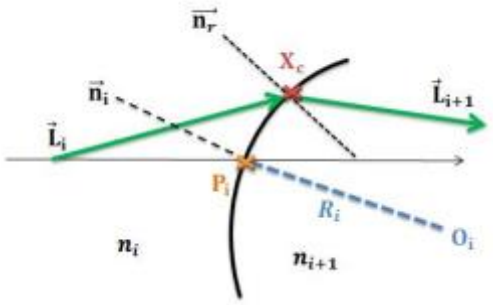

Fig. 2. Details of interaction of a photon with i^{th} boundary

To obtain $\vec{\mathbf{L}}_\mathbf{i+1}$, three equations which are derived based on Eq. (3) are,

$$c_r\mu_y' - b_r\mu_z' = \frac{n_i}{n_{i+1}}(c_r\mu_y - b_r\mu_z), \quad \textbf{(12)}$$

$$c_r\mu_x' - a_r\mu_z' = \frac{n_i}{n_{i+1}}(c_r\mu_x - a_r\mu_z), \quad \textbf{(13)}$$

$$b_r\mu_x' - a_r\mu_y' = \frac{n_i}{n_{i+1}}(b_r\mu_x - a_r\mu_y). \quad \textbf{(14)}$$

It is concluded from Eq. (12), (13) and (14) that

$$\mu_y' = \frac{b_r \mu_x' - (b_r \mu_x - a_r \mu_y)}{a_r}, \quad (15)$$

$$\mu_z' = \frac{c_r \mu_x' - (c_r \mu_x - a_r \mu_z)}{a_r}. \quad (16)$$

Substituting Eq. (15) and (16) in Eq. (8), μ_x' is obtained by,

$$\mu_x'^2 + 2\mu_x' [a_r (\vec{n_r}.\vec{L_i}) - \mu_x] - 2\mu_x a_r (\vec{n_r}.\vec{L_i}) + \mu_x^2 = 0. \quad (17)$$

Eq. (17) will results in two solutions: (*i*) omitted photon's direction toward Tx; and (*ii*) correct photon's direction toward the Rx.

Due to small incident angles adopted throughout the simulation, both the reflection and the total internal reflection between layers have not been considered for simplicity. At every interaction of a photon with the medium, both their current position and direction are updated. These attributes are recorded and are used to make decision on which photon is received. Note that, only the photons within the Rx aperture and with polar angles ($\cos^{-1}\mu_z$) less than the half angle of Rx FOV are selected as detected photons.

4. RESULTS

A. Simulation methodology

The simulation is implemented using MATLAB. To determine the received optical intensity fluctuations, we used a specific number of transmitted photons for 1000 channel realizations with each representing a time sample of the channel. In each channel realization, n_i, R_i, θ_i and φ_i related to each boundary are selected randomly from uniform distributions within their specified domains. These sets of random numbers are changing in each channel realizations to implement the chaotic characteristics of the turbulent time-variant channel.

The received optical power values are obtained for all channel realizations based on the total number of received photons, which are normalized to the average received powers and the corresponding PDF is plotted such that the area under it equals to unity. The SI is obtained from the following equation, in that I is the received intensity,

$$\sigma_I^2 = \frac{\langle I^2 \rangle - \langle I \rangle^2}{\langle I \rangle^2}. \quad (18)$$

B. PDF distributions

Here, we have adopted the two well-known PDF distributions of received intensity fluctuations of lognormal and negative exponential for weak and saturation turbulence regimes, respectively. The lognormal distribution for a Gaussian beam is given by [36],

$$p(I) = \frac{1}{I\sigma_I\sqrt{2\pi}} \exp\left\{ -\frac{\left[\ln(\frac{I}{I_0}) + \frac{1}{2}\sigma_I^2\right]^2}{2\sigma_I^2} \right\}, I > 0 \quad (19)$$

where I_0 is the mean received light intensity. In the limit of strong intensity fluctuations in the saturation turbulence regime where SI~1 [21], negative exponential distribution is given by,

$$p(I) = \frac{1}{I_0} \exp(-\frac{1}{I_0}), I > 0 \quad (20)$$

Other PDF distributions such as log-normal-Rician, I-K, K and gamma-gamma distributions all reduce to the negative exponential in the limit of strong turbulence and therefore are not considered here [21].

C. Experimental verification

In this section we verify the proposed simulation model by means of experimental investigation based on the work reported in [23] under weak turbulence. In [23] a laser light source at a wavelength and power of 632 nm and 1.5 mW, respectively, CMOS camera and 1 m long plexiglass tank were used to obtain the PDF of intensity fluctuations. To compare our result with their experimental data specifically, we consider part of the test which turbulence was created on distilled water with temperature gradient and with no particles and no scattering with the reported SI of 11e-4.

According to the reported information [23], we assumed no salinity and pressure, and used temperature variation in the range of 20-20.2° C, λ of 632 nm, and a link span of 1 m to obtain the refractive index variation Δn=[1.3317-1.3318]. The distance between successive layers Δz is equal to 0.05 m and R_i is within the range of 0.05-1 m. Note that, θ_{max} is 15° and φ_i is chosen randomly in the interval of [0, 2π]. The size of the receiver's aperture was assumed to be 2 mm. Using the given parameters, we determined a SI of 19e-4. Fig. 3 shows the PDF for lognormal as well as data for simulated and experimental (from [23]) PDFs. Note that, there is a good match between the simulated and experimental data except around the peak points.

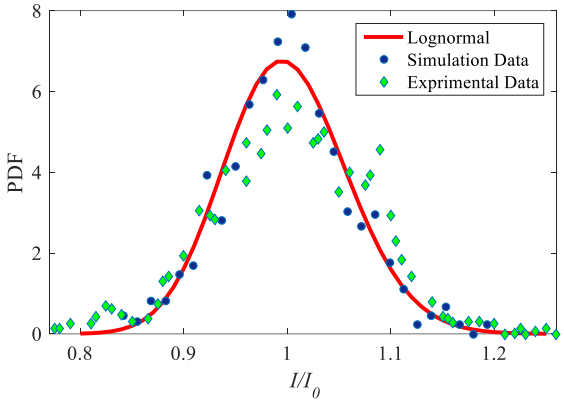

Fig. 3. Simulation data fitted with experimental data and lognormal PDF distribution

D. PDF of simulation intensity fluctuations

We present here the PDF of simulated intensity for the weak, moderate-to-strong and saturation turbulence regimes using the parameters given in Table 1.

It was reported in [12] that the inertial scale of turbulent cells could be in the order of centimeters to ensure locally isotropic and homogenous turbulence. In our model we set the distance between successive layers Δz to 50 cm. R_i is chosen randomly in the range of 0.5-10 m from a uniform distribution to cover all possible cases of turbulent cells. θ_{max} is 45° and φ_i is chosen randomly in the interval of [0, 2π] in a 200 m link span.

To change the distribution of n for each simulation scenario, m values of n_i are chosen randomly in the interval of $[N_{avg} - \Delta n/2, N_{avg} + \Delta n/2]$ where N_{avg} is the average of maximum variation of n [1.3412, 1.3420]. Δn is defined separately for each scenario [28].

Table 1. Simulation Parameters

Parameter	Value
λ	520 nm
T	23-29◦ C
S	36.1-36.8 ppm
P	0-10 dbar
Maximum Δn	0.0008
Link span	200 m
Laser beam divergence (half angle)	0.00075 rad
Beam width	15 mm
Rx aperture diameter	100 mm
Number of transmitted photons	1e4
Number of channel realizations	1e3
Δz	50 cm
$\boldsymbol{R_i}$	0.5-10 m
Number of layers	400
$\boldsymbol{\theta_{max}}$	45˚

Here, the focus is on the effect of variation of n on the intensity fluctuations, which results in different turbulence regimes. Figs. 4 (a) and (b) depicts PDF of simulation data and lognormal as a function of normalized I for Δn of 16e-7, and 8e-5, which result in SI of 0.001, and 0.0022, respectively. In both figures, there is a good match between lognormal and the simulated data under weak turbulence. For higher values of Δn i.e., 6e-5 and 40e-5, which results in SI of 0.01 and 0.2, the PDF plots are illustrated in Figs. 5 (a) and (b), respectively. As can be seen for the moderate-to-strong turbulence regime the simulated data profile is no longer the same as lognormal. In this turbulence regime, we could not find any known distribution to be fitted to the simulation data. Such results are however, potentially useful in the communications system design and they are testable predictions that could motivate future efforts to improve and extend experimental techniques and observations. As Δn increases even more i.e., 64e-5 and 80e-5, which results in SI of 0.7 and, 1.2 in Figs. 6 (a) and (b), respectively, the simulated data fits well with the negative exponential distribution under the strong-to-saturation turbulence regime.

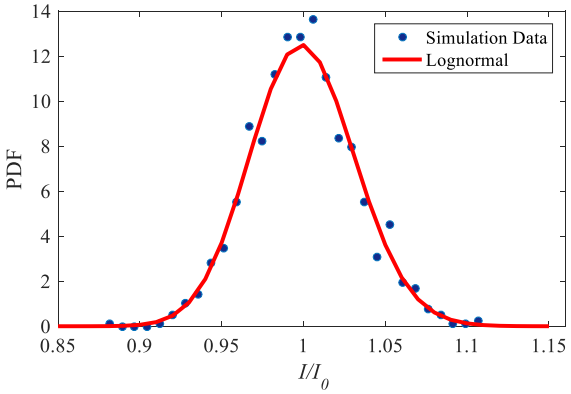

(a)

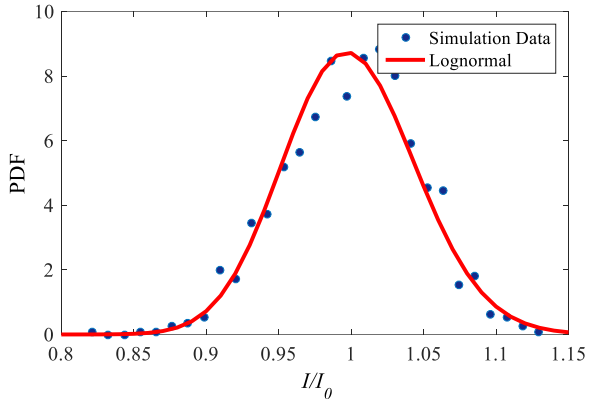

(b)

Fig. 4. PDF of simulation data and lognormal for Δn of: (a) 16e-7 (SI of 0.001), and (b) 8e-5 (SI of 0.0022)

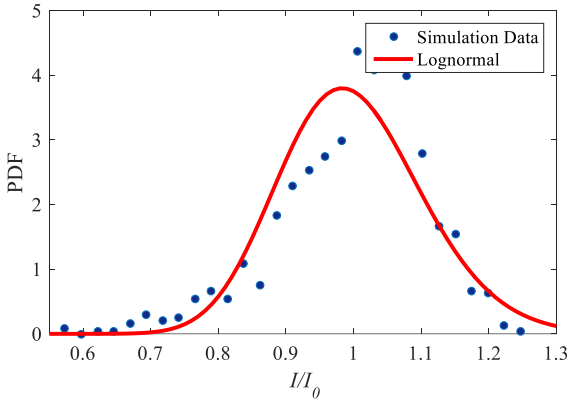

(a)

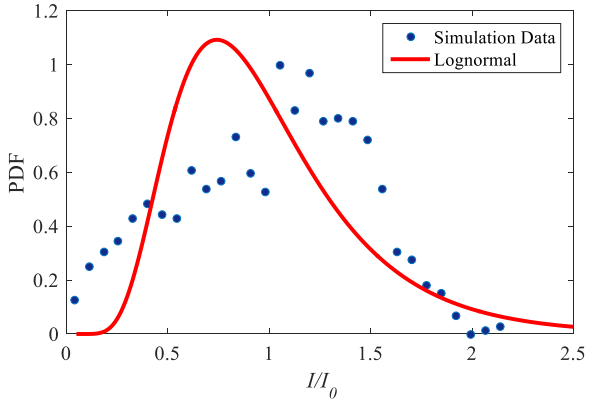

(b)

Fig. 5. PDF of simulation data and lognormal for Δn of: (a) 6e-5 (SI of 0.01), and (b) 40e-5 (SI of 0.2)

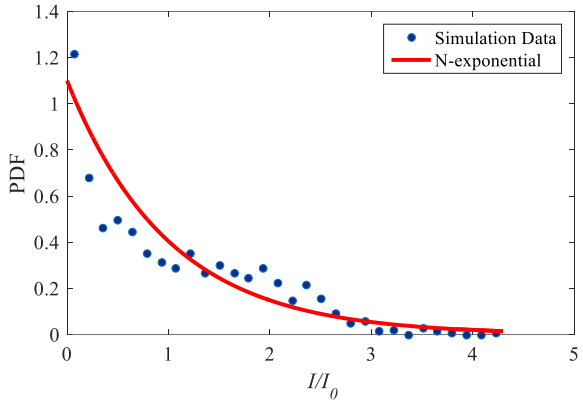

(a)

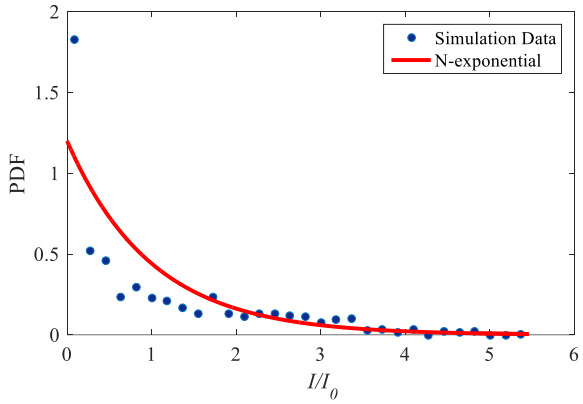

(b)

Fig. 6. PDF of simulation data and negative exponential for Δ*n* of: (a) 64e-5 (SI of 0.7), and (b) 80e-5 (SI of 1.2)

To evaluate how well the simulation data fit with lognormal and negative exponential distributions, the determination coefficient R^2 is examined for the weak and saturation turbulence regimes as given by,

$$R^2 = 1 - \frac{\sum_{i=1}^{N}(x_i - y_i)^2}{\sum_{i=1}^{N}(x_i - \bar{x})^2}, 0 < R^2 < 1 \quad \textbf{(21)}$$

where N is the number of bins in the obtained simulation distribution, x_i and y_i are the simulated and predicted values for the i^{th} intensity bin, respectively, and $\bar{x}$ is the average of x_i for the i^{th} intensity bin [37]. Table 2 shows R^2 values for a range of SI and lognormal and negative exponential PDFs, which illustrate that the best fit is with lognormal for weak turbulence. The low values of fit in the negative exponential is due to the zero intensity bin, where the simulated data cannot be predicted well enough as a result of the deficiency of the model for the saturation turbulence regime.

Table 2. R^2 of Simulated PDF for Weak and Saturation Turbulence Regimes

SI	PDF	R^2
0.001	Lognormal	0.9546
0.0022	Lognormal	0.9018
0.7	N-exponential	0.8612
1.2	N-exponential	0.7298

E. Scintillation index and turbulence induced path loss

The SI and average received power as function of the link span L for a range of Δn are presented in Figs. 7 (a) and (b), respectively. Fig. 7 (a) shows that the SI increases with L as was reported in previous works based on the parameters of Kolmogorov power spectrum [14, 15], but not considering Δn. In Fig. 7 (b) the predicted power loss with no turbulence (i.e., Δn=0) is due to the diffraction of Gaussian beam. However, as Δn increases, especially in longer transmission spans, the link experience more turbulence induced losses. This is due to the spreading effect of n fluctuations in turbulent water [9].

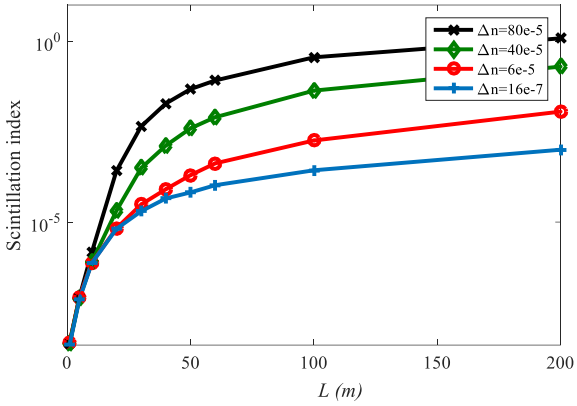

(a)

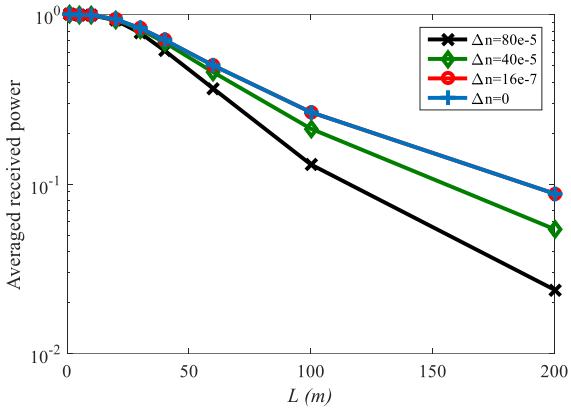

(b)

Fig. 7. (a) Scintillation index vs. the link span, and (b) turbulence induced path loss for a range of Δn

5. CONLCUSION

Despite the previous methods to model multiple scattering and absorption effect, a physical simulation model is needed to investigate the influence of turbulence in UWOC applications thoroughly. To achieve this goal, in this paper, a novel turbulence model based on the Monte Carlo simulation method was presented for UWOC application. The offered simulation model that is based on the refractive index variation is simple and flexible on the contrary to the CFD simulation tools. The model was simulated in weak, moderate-to-strong and saturation turbulence regimes to obtain the PDF of intensity fluctuations. Simulation distributions in weak turbulence were fitted with lognormal PDF and they were in accordance with the previous experimental work. In saturation regime, the negative exponential was fitted satisfactory with the simulation distributions as predicted and experimentally tested in atmospheric turbulence. The shapes of the PDF obtained from our simulation model for moderate-to-strong

turbulent regime have not been predicted by theory nor are experimental observation readily available and we could not find a previously known PDF distribution for them. Furthermore, for the first time we presented the scintillation index and the turbulence induced path loss versus the link span for different refractive index variations.

References

1. Z. Zeng, "A survey of underwater wireless optical communication," (University of British Columbia, 2015).
2. B. M. Cochenour, L. J. Mullen, and A. E. Laux, "Characterization of the beam-spread function for underwater wireless optical communications links," IEEE J. of Oceanic Engineering **33**, 513-521 (2008).
3. C. Gabriel, M. A. Khalighi, S. Bourennane, P. Léon, and V. Rigaud, "Monte-carlo-based channel characterization for underwater optical communication systems," J. Opt. Commun. Netw. **5**, 1-12 (2013).
4. S. Tang, Y. Dong, and X. Zhang, "Impulse response modeling for underwater wireless optical communication links," IEEE Transactions on Communications **62**, 226-234 (2014).
5. W. Cox and J. Muth, "Simulating channel losses in an underwater optical communication system," J. Opt. Soc. Am. A **31**, 920-934 (2014).
6. S. Q. Duntley, "Light in the sea," J. Opt. Soc. Am. **53**, 214-233 (1963).
7. G. D. Gilbert, T. R. Stoner, and J. L. Jernigan, "Underwater experiments on the polarization, coherence, and scattering properties of a pulsed blue-green laser," Proc. SPIE **0007**, 8-14 (1966).
8. S. Tang, X. Zhang, and Y. Dong, "Temporal statistics of irradiance in moving turbulent ocean," in *OCEANS - Bergen, MTS/IEEE* (IEEE, 2013), pp. 1-4.
9. L. C. Andrews and R. L. Phillips, *Laser Beam Propagation Through Random Media* (SPIE, 2005).
10. F. Hanson and M. Lasher, "Effects of underwater turbulence on laser beam propagation and coupling into single-mode optical fiber," Appl. Opt. **49**, 3224-3230 (2010).
11. W. Hou, S. Woods, E. Jarosz, W. Goode, and A. Weidemann, "Optical turbulence on underwater image degradation in natural environments," Appl. Opt. **51**, 2678-2686 (2012).
12. G. Nootz, E. Jarosz, F. R. Dalgleish, and W. Hou, "Quantification of optical turbulence in the ocean and its effects on beam propagation," Appl. Opt. **55**, 8813-8820 (2016).
13. W. Liu, Z. Xu, and L. Yang, "SIMO detection schemes for underwater optical wireless communication under turbulence," Photon. Res. **3**, 48-53 (2015).
14. O. Korotkova, N. Farwell, and E. Shchepakina, "Light scintillation in oceanic turbulence," Waves in Random and Complex Media **22**, 260-266 (2012).
15. H. Gerçekcioğlu, "Bit error rate of focused Gaussian beams in weak oceanic turbulence," J. Opt. Soc. Am. A **31**, 1963-1968 (2014).
16. Y. Ata and Y. Baykal, "Scintillations of optical plane and spherical waves in underwater turbulence," J. Opt. Soc. Am. A **31**, 1552-1556 (2014).
17. Y. Baykal, "Higher order mode laser beam scintillations in oceanic medium," Waves in Random and Complex Media **26**, 21-29 (2016).
18. S. A. Arpali, Y. Baykal, and Ç. Arpali, "BER evaluations for multimode beams in underwater turbulence," Journal of Modern Optics **63**, 1297-1300 (2016).
19. M. C. Gökçe and Y. Baykal, "Scintillation analysis of multiple-input single-output underwater optical links," Appl. Opt. **55**, 6130-6136 (2016).
20. F. S. Vetelino, C. Young, L. Andrews, and J. Recolons, "Aperture averaging effects on the probability density of irradiance fluctuations in moderate-to-strong turbulence," Appl. Opt. **46**, 2099-2108 (2007).
21. Z. Ghassemlooy, W. Popoola, and S. Rajbhandari, *Optical Wireless Communications: System and Channel Modelling with MATLAB* (CRC Press, Inc., 2012).
22. M. P. Bernotas and C. Nelson, "Probability density function analysis for optical turbulence with applications to underwater communications systems," Proc. SPIE **9827** (2016).
23. M. Bernotas and C. Nelson, "Probability density function analysis for optimization of underwater optical communications systems," in *OCEANS'15 MTS/IEEE Washington* (IEEE, 2015), pp. 1-8.
24. X. Yi, Z. Li, and Z. Liu, "Underwater optical communication performance for laser beam propagation through weak oceanic turbulence," Appl. Opt. **54**, 1273-1278 (2015).
25. A. C. Boucouvalas, K. P. Peppas, K. Yiannopoulos, and Z. Ghassemlooy, "Underwater optical wireless communications with optical amplification and spatial diversity," IEEE Photonics Technology Letters **28,** 2613-2616 (2016).
26. Y. Dong and J. Liu, "On BER performance of underwater wireless optical MISO links under weak turbulence," in *OCEANS 2016 - Shanghai* (IEEE, 2016), pp. 1-4.
27. M. V. Jamali, F. Akhoundi, and J. A. Salehi, "Performance characterization of relay-assisted wireless optical CDMA networks in turbulent underwater channel," IEEE Transactions on Wireless Communications **15**, 4104-4116 (2016).
28. V. V. Nikishov and V. I. Nikishov, "Spectrum of turbulent fluctuations of the sea-water refraction index," Inter. J. Fluid. Mech. Res. **27**, 82-98 (2000).
29. N. Farwell, "Optical beam propagation in oceanic turbulence," (University of Miami, 2014).
30. S. A. Thorpe, *An Introduction to Ocean Turbulence* (Cambridge University Press, 2007).
31. L. Sun, J. Wang, K. Yang, M. Xia, and J. Han, "The research of optical turbulence model in underwater imaging system," Sensors & Transducers **163**, 107-112 (2014).
32. R. C. Millard, and G. Seaver, "An index of refraction algorithm for seawater over temperature, pressure, salinity, density, and wavelength," Deep Sea Research Part A. Oceanographic Research Papers **37**, 1909-1926 (1990).
33. M. Jonasz, and G. R. Fournier, *Light Scattering by Particles in Water: Theoretical and Experimental Foundations* (Academic Press, 2011).
34. S. Matt, W. Hou, W. Goode, and S. Hellman, "Velocity fields and optical turbulence near the boundary in a strongly convective laboratory flow," Proc. SPIE **9827** , 1-11 (2016).
35. C. D. Mobley, *Light and Water: Radiative Transfer in Natural Waters* (Academic Press, 1994).
36. L. C. Andrews, R. L. Phillips, and C. Y. Hopen, *Laser Beam Scintillation with Applications* (SPIE Press, 2001).
37. I. E. Lee, "Free-space optical communication systems with a partially coherent gaussian beam and media diversity," (University of Northumbria, Newcastle, 2014).